



## Crack path predictions and experiments in plane structures considering anisotropic properties and material interfaces

P.O. Judt, A. Ricoeur

University of Kassel, Institute of Mechanics, 34125 Kassel, Germany  
judt@uni-kassel.de, ricoeur@uni-kassel.de

**ABSTRACT.** In many engineering applications special requirements are directed to a material's fracture behavior and the prediction of crack paths. Especially if the material exhibits anisotropic elastic properties or fracture toughnesses, e.g. in textured or composite materials, the simulation of crack paths is challenging. Here, the application of path independent interaction integrals ( $I$ -integrals),  $J$ -,  $L$ - and  $M$ -integrals is beneficial for an accurate crack tip loading analysis.

Numerical tools for the calculation of loading quantities using these path-invariant integrals are implemented into the commercial finite element (FE)-code ABAQUS. Global approaches of the integrals are convenient considering crack tips approaching other crack faces, internal boundaries or material interfaces. Curved crack faces require special treatment with respect to integration contours. Numerical crack paths are predicted based on FE calculations of the boundary value problem in connection with an intelligent adaptive re-meshing algorithm. Considering fracture toughness anisotropy and accounting for inelastic effects due to small plastic zones in the crack tip region, the numerically predicted crack paths of different types of specimens with material interfaces and internal boundaries are compared to subcritically grown paths obtained from experiments.

**KEYWORDS.**  $J$ -,  $M$ -,  $L$ -integral; Interaction integral; Fracture toughness anisotropy; Material interfaces; Crack paths; Fracture process zone.

### INTRODUCTION

For the sake of an accurate prediction of crack paths, the loading analysis at cracks is one crucial part of the model. Here, the application of path-independent integrals with remote integration contours is beneficial compared to local approaches, as no special requirements regarding the crack tip meshing have to be considered. Integrating along large contours far from the crack tip essentially exploits numerically reliable data.

The theory of forces at defects and singularities was established by Eshelby [1] and applied to cracks and notches by Cherepanov [2] and Rice [3], introducing the path-independent  $J$ -integral. Investigations by Günther [4] and Knowles and Sternberg [5] provided balance equations including the  $J$ -,  $M$ - and  $L$ -integrals, which were generalized to linear elastic fracture mechanics (LEFM) by Budiansky and Rice [6]. Later these balance laws founded the theory of the material or configurational forces [7].

In LEFM, the  $J_k$ -integral vector, representing the crack driving force, is related to the stress intensity factors (SIF) [8] and the energy release rate (ERR). Large integration contours at curved cracks require the integration along crack faces,



providing numerically inaccurate values approaching the crack tip, finally leading to large deviations in  $J_2$ . Improvements for an accurate calculation of  $J_2$  have been presented by Eischen [9] and Judt and Ricoeur [10].

The interaction integral or  $I$ -integral is another conservation integral of the  $J$ -integral type [11]. Here, the interaction of the physical and an auxiliary crack tip loading is used for the direct calculation of SIF. In general, auxiliary fields are obtained from the asymptotic near tip solution for stresses and displacements. Considering curved cracks, the jump of the auxiliary fields represents the straight auxiliary crack, introducing another strong discontinuity.

Calculating the global  $I$ -integral, path-independence is maintained considering the integration along both physical and auxiliary crack faces [12]. Due to the fact that the auxiliary fields may be chosen arbitrarily, just satisfying balance, constitutive and kinematic laws, the  $I$ -integral can be applied to elegant analyzing multiple cracks systems [13].

The  $M$ - and  $L$ -integrals are akin to the  $J$ -integral and, in terms of the concept of material forces, represent the scalar moment and vector moment induced by the crack driving force. Especially if multiple defects are considered, these integrals provide a distinction between the crack driving force and other material forces [14]. In the paper this concept is adopted for a separation of the crack driving force and the forces acting in the plastic deformation.

For an accurate calculation of crack paths, the anisotropic elastic and fracture mechanical properties must also be considered in the model. The elastic anisotropy is related to the crack tip loading analysis [15], whereas the fracture toughness anisotropy requires an extended theory for determining the crack deflection angle [16].

Material interfaces and internal boundaries represent inhomogeneities in the material space, thus producing configurational forces along these boundaries. To obtain the crack driving force, the integration along these boundaries is necessary, providing path-independence. This paper presents a numerical model for the accurate loading analysis and crack path prediction considering anisotropic properties and material interfaces. Calculated crack paths are presented and compared to those obtained from crack growth experiments.

## THEORY OF PATH-INDEPENDENT INTEGRALS

The Lagrangian density of a system exhibiting a potential  $U$  is defined as  $\mathcal{L} = T - U$ , with  $T$  being the kinetic density. The balance laws in the configurational space are derived from applying the **gradient, divergence** and **curl** operator to the Lagrangian  $\mathcal{L}$  and the Lagrangian moment  $\mathcal{L}x_k$  [17]. Assuming quasi-static conditions, material isotropy and homogeneity, thus neglecting an explicit dependence of  $\mathcal{L}$  on the location  $x_k$ , the balance laws read

$$\text{grad}(\mathcal{L}) \rightarrow [U\delta_{kj} - \sigma_{ij}u_{i,k}]_{,j} = Q_{kj,j} = 0 \quad (1)$$

$$\text{div}(\mathcal{L}\mathbf{x}) \rightarrow \left[ Q_{kj}x_k + \left(1 - \frac{m}{2}\right)\sigma_{ij}u_i \right]_{,j} = Q_{kj,j}x_k = 0, \quad (2)$$

$$\text{curl}(\mathcal{L}\mathbf{x}) \rightarrow \epsilon_{mkn} [Q_{kj}x_n + \sigma_{kj}u_n]_{,j} = \epsilon_{mkn}Q_{kj,j}x_n = 0, \quad (3)$$

with  $Q_{kj}$  being Eshelby's energy-momentum tensor,  $\delta_{kj}$  Kronecker's identity tensor,  $\epsilon_{mkn}$  the Levi-Civita symbol,  $\sigma_{ij}$  the stress tensor,  $u_i$  the displacements and  $m = 2$  in two-dimensional and  $m = 3$  in three-dimensional space. Eqs. (1) - (3) represent balance equations in a defect-free material. Applying these laws to boundary value problems including a crack, the integrals of a domain  $V$  provide finite values and are denoted as  $J_k$ -,  $M$ - and  $L_m$ -integrals. Considering plane problems, i.e.  $m = 2$ , and  $L = L_3$  in the following, the integrals are transformed with Gauss' theorem into line integrals, surrounding the defect or the crack tip, see Fig. 1(a), now reading

$$J_k = \lim_{\epsilon \rightarrow 0} \int_{\Gamma_\epsilon} Q_{kj}n_j d\mathbf{s}, \quad (4)$$

$$M = \lim_{\epsilon \rightarrow 0} \int_{\Gamma_\epsilon} (Q_{kj}x_k)n_j d\mathbf{s} = \lim_{\epsilon \rightarrow 0} \int_{\Gamma_\epsilon} Q_{kj}n_j d\mathbf{s} x_k = J_k x_k, \quad (5)$$

$$L = \lim_{\epsilon \rightarrow 0} \int_{\Gamma_\epsilon} \epsilon_{kn} \left( Q_{kj} x_n + \sigma_{kj} u_n \right) n_j ds = \epsilon_{kn} \lim_{\epsilon \rightarrow 0} \int_{\Gamma_\epsilon} Q_{kj} n_j ds x_n = \epsilon_{kn} J_k x_n, \quad (6)$$

if the contour  $\Gamma_\epsilon$  is shrunk to the crack tip. A reduced notation  $\epsilon_{3kn} = \epsilon_{kn}$  is introduced for the Levi-Civita symbol. Applying finite integration contours and considering curved cracks and mixed-mode loading, integration along the crack faces is required to provide path-independence. Special treatment is necessary for the accurate calculation of  $J_2$  and  $L$ . Here, numerical inaccuracies are adjusted, e.g. extrapolating the non-singular part of tangential stresses on the crack faces towards the crack tip [10].

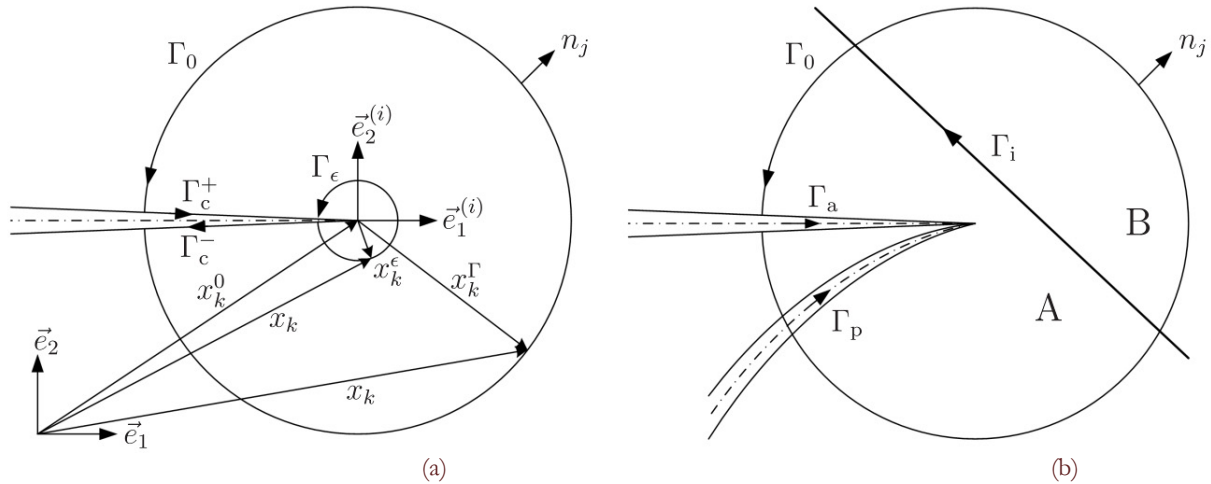


Figure 1: Integration contours, for path-independent  $J_k$ -,  $M$ -,  $L$  and  $I_k$ -integrals, considering physical ( $\Gamma_p$ ) and auxiliary ( $\Gamma_a$ ) crack faces and a material interface ( $\Gamma_i$ ).

The  $M$ - and  $L$ -integrals depend on the origin of the global coordinate system  $\vec{e}_k$ . From Eqs. (5) and (6) and from Fig. 1(a) it becomes clear that if the global coordinate system coincides with the crack tip coordinate system  $\vec{e}_k^{(i)}$ ,  $M$ - and  $L$ -integrals vanish as  $x_k^\epsilon \rightarrow 0$ . Otherwise, if the vector  $x_k^0$  is pointing from the origin of the global frame to the crack tip and thus  $x_k = x_k^0 + x_k^\epsilon$ ,  $M$ - and  $L$ -integrals are finite and represent the scalar and vector moments induced by the crack driving force  $J_k$ . This feature can be applied to the separation of crack tip loadings in two-cracks systems by a global approach, i.e. by calculating the integrals along remote contours including both crack tips [14].

The  $I_k$ -integral represents the interaction of two loading scenarios at a crack, i.e. the physical (a) and an auxiliary (b) loading [11].  $I_k$  is derived by substituting the superimposed stress and displacement fields  $u_i^{(a)+(b)} = u_i^{(a)} + u_i^{(b)}$  and  $\sigma_{ij}^{(a)+(b)} = \sigma_{ij}^{(a)} + \sigma_{ij}^{(b)}$  into Eq. (4), yielding  $J_k^{(a)+(b)} = J_k^{(a)} + J_k^{(b)} + I_k$ . With the interaction energy-momentum tensor  $Q_{kj}^{(a/b)}$  the  $I_k$ -integral reads

$$I_k = \lim_{\epsilon \rightarrow 0} \int_{\Gamma_\epsilon} \left[ \frac{1}{2} \left( \sigma_{mn}^{(a)} \epsilon_{mn}^{(b)} + \sigma_{mn}^{(b)} \epsilon_{mn}^{(a)} \right) \delta_{kj} - \left( \sigma_{ij}^{(a)} u_{i,k}^{(b)} + \sigma_{ij}^{(b)} u_{i,k}^{(a)} \right) \right] n_j ds = \lim_{\epsilon \rightarrow 0} \int_{\Gamma_\epsilon} Q_{kj}^{(a/b)} n_j ds. \quad (7)$$

Applying finite integration contours, the integration along both the physical ( $\Gamma_p$ ) and the auxiliary ( $\Gamma_a$ ) crack faces is required to provide path-independence [12]. If material interfaces are considered, e.g.  $\Gamma_i$  between material A and B in Fig. 1(b), integration along the interfaces is required in Eqs. (4) - (7) for the sake of path-independence.  $J_k$ - and  $I_k$ -integrals accounting for crack face and interface integrals read

$$J_k = \int_{\Gamma_0} Q_{kj} n_j ds + \int_{\Gamma_p} \left[ \left[ Q_{kj} \right] \right]_+ n_j ds + \int_{\Gamma_i} \left[ \left[ Q_{kj} \right] \right]_B^A n_j ds, \quad (8)$$



$$I_k = \int_{\Gamma_0} \mathcal{Q}_{kj}^{(a/b)} n_j ds + \int_{\Gamma_p} \left[ \left[ \mathcal{Q}_{kj}^{(a/b)} \right] \right]_+ n_j ds + \int_{\Gamma_a} \left[ \left[ \mathcal{Q}_{kj}^{(a/b)} \right] \right]_- n_j ds + \int_{\Gamma_i} \left[ \left[ \mathcal{Q}_{kj}^{(a/b)} \right] \right]_B^\Lambda n_j ds, \quad (9)$$

and  $\left[ \left[ \mathcal{Q}_{kj} \right] \right]$  denotes the jump of the energy-momentum tensor across crack faces and interfaces. A local coordinate system  $\bar{e}_k^*$  is introduced, with  $\bar{e}_1^*$  pointing into the tangential direction of the interface. The stress vector  $t_i$  and the tangential derivatives of displacements  $u_{i,1}$  are continuous at the interface. The integrand related to the  $J_k$ -integral reads

$$\left[ \left[ \mathcal{Q}_{2j} \right] \right]_B^\Lambda n_j = -\frac{1}{2} \left[ \left( \sigma_{11}^{(A)} - \sigma_{11}^{(B)} \right) u_{1,1}^{(AB)} - \sigma_{12}^{(AB)} \left( u_{1,2}^{(A)} - u_{1,2}^{(B)} \right) - \sigma_{22}^{(AB)} \left( u_{2,2}^{(A)} - u_{2,2}^{(B)} \right) \right], \quad (10)$$

with (AB) denoting values that are continuous across the material interfaces. The additional integrand related to the  $I_k$ -integral reads

$$\left[ \left[ \mathcal{Q}_{2j}^{(a/b)} \right] \right]_B^\Lambda n_j = -\left[ \left( \sigma_{11}^{(b,A)} - \sigma_{11}^{(b,B)} \right) u_{1,1}^{(a,AB)} - \sigma_{12}^{(a,AB)} \left( u_{1,2}^{(b,A)} - u_{1,2}^{(b,B)} \right) - \sigma_{22}^{(a,AB)} \left( u_{2,2}^{(b,A)} - u_{2,2}^{(b,B)} \right) \right]. \quad (11)$$

Bearing in mind that the auxiliary fields do not have to exhibit an interface, an appropriate choice is (b, A) = (b, B), providing  $\left[ \left[ \mathcal{Q}_{2j}^{(a/b)} \right] \right]_B^\Lambda n_j = 0$ . Therefore, according to Yu et al. [18], the integration along the interface should be superfluous. Our investigations reveal, however, that the integral along the interface according to Eq. (9) must not be neglected. Path-independence is investigated at a model with a straight slant crack, hole and interface as presented by Judt and Ricoeur [19], where the values  $J_2$  were obtained without special treatment of the crack face integrals [10] thus being inaccurate. The  $J_k$ - and  $I_k$ -integrals along small circular contours enclosing the crack tip (denoted as local) are compared to the values obtained by the approach as presented in this section according to Eqs. (8) and (9) (denoted as global). Furthermore, SIF are calculated for a comparison of  $J_k$ - and  $I_k$ -integrals. Three different choices of the auxiliary fields are considered in the region B (see Fig. 1(b)):

- a) the auxiliary fields are chosen according to the material constants in B, respectively;
- b) the auxiliary fields are chosen according to the material constants in A and the integration along the interface is neglected in Eq. (9);
- c) the auxiliary fields are chosen according to the material constants in A and the  $I_k$ -integral is calculated according to Eq. (9).

Method	$J_I$ or $I_I$ / (N/mm)	$J_2$ or $I_2$ / (N/mm)	$K_I$ / MPa√mm	$K_{II}$ / MPa√mm
$J_k$ local	0.05721	-0.03304	104.46	33.21
$J_k$ global	0.05731	-0.03301	104.58	33.15
$I_k$ local	0.0009954	-0.0003162	104.52	33.21
$I_k$ global (a)	0.0009948	-0.0003168	104.46	33.27
$I_k$ global (b)	0.0008242	-0.0004517	86.54	47.43
$I_k$ global (c)	0.0009725	-0.0003119	102.12	32.75

Table 1: Numerical values of local and global  $J_k$ - and  $I_k$ -integrals and SIF, three different choices of the auxiliary fields **a – c**.

From the results in Tab. 1 it is obvious that path-independence is only retained considering interface integrals. Nevertheless, values for the non-physical choice of the auxiliary fields differ slightly from those of the physically motivated choice with dissimilar elastic constants in A and B.

## ANISOTROPY IN ELASTIC PROPERTIES AND FRACTURE TOUGHNESS

The extrusion, drawing or rolling process applied to wrought metal products, in general yields a specified geometric orientation of the microstructure (texture) and thus of the material's mechanical properties. The  $J_k$ -integral according to Eq. (8) may be applied straight forwardly to anisotropic elastic material [15]. As the near-tip stress

and displacement fields differ from the isotropic case, the relation between  $J_k$ -integral and SIF must be adapted. Furthermore, due to the rolling process, anisotropic fracture toughness is observed. In plates of Al-7075-T651, the crack resistance in the rolling direction (RD) is smaller than in the transverse direction (TD),  $G_c^{RD} < G_c^{TD}$ , thus depending on the global angle  $\alpha$ . The crack resistance anisotropy is accounted for in the fracture criterion by introducing an elliptic interpolation function  $G_c(\alpha)$ . The ERR is the projection of the  $J_k$ -vector onto the crack growth direction and thus can be written as a function of  $\alpha$ . Finally, the maximum value of the ratio  $G_R = G(\alpha) / G_c(\alpha)$  provides the crack deflection angle. In rolled plates of Al-7075-T651, the anisotropy of the crack resistance is measured by standard CT tests providing  $G_c^{RD} = 9.0 \text{ N/mm}$  and  $G_c^{TD} = 11.4 \text{ N/mm}$ . The ratio of fracture toughness anisotropy, i.e.  $\chi = \sqrt{G_c^{TD} / G_c^{RD}} = 1.12$  for this material, is an important parameter of the model and must be considered for the correct prediction of crack paths [16].

### CRACK PATH PREDICTION

The presented model is applied for the prediction of crack paths at specimens with material interfaces. The specimen is cut from a rolled plate of aluminum alloy Al-7075-T651 (Young's modulus  $E = 72000 \text{ MPa}$ , Poisson's ratio  $\nu = 0.3$ ) and exhibits a circular hole. The incipient crack, exhibiting a length of  $a_0 = 13.5 \text{ mm}$ , is aligned parallel to the TD. A cylindrical steel core (steel 9S20K, Young's modulus  $E = 210000 \text{ MPa}$ , Poisson's ratio  $\nu = 0.3$ ) is grouted into the hole leading to an initial stress distribution at the interface region, see Fig. 2(b). The hole's diameter is  $d = 22 \text{ mm}$  and the diameter of the steel core is slightly larger. The clamping of the steel core leads to an initial stress distribution at the interface region. The calculation procedure involves an intelligent remeshing algorithm refining the mesh at the crack faces and tip, and a repeated incremental extension of the crack. The crack extension parameter is chosen  $\Delta a = 0.5 \text{ mm}$ . A numerical loading analysis is performed applying remote integration contours according to Section 2, providing the  $J_k$ -integral after each crack extension step. The crack deflection angle is calculated according to Section 3. Further details are presented in [16]. Three configurations of the model with different boundary conditions at the hole are investigated in the simulation and compared with the experiment. In configuration 1 the phase B is just air, the hole representing a free boundary. The configuration 2 considers the material B to be a steel core which is perfectly bonded to the aluminum specimen. In the configuration 3 the material B also represents a steel core, which is grouted into the hole allowing for a separation of the materials A and B. To provide path independence of the  $J_k$ -integral, the integration along the hole  $\Gamma_h$  is considered, see Fig. 2(b). The calculated crack paths reveal that the impressed steel core, according to configuration 3, attracts the crack even stronger than solely a hole with free surfaces (configuration 1). In contrast to configuration 3 a perfectly bonded steel core induces the crack to veer away from the core. Similar results as observed at configuration 2 have been reported by Patton and Santare [20], Bouchard et al. [21] and Nielsen et al. [22]. The crack path obtained from the experiment, where the boundary conditions of configuration 3 are met, is in very good agreement with the numerically predicted path. At the beginning, the crack veers away from the steel core and is then strongly attracted finally ending in the hole.

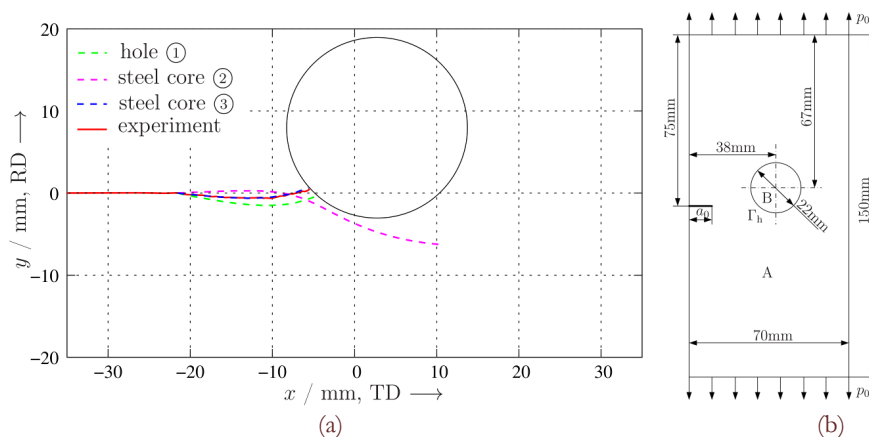


Figure 2: (a) Comparison of experimental and numerically predicted crack paths for three different model configurations, (b) aluminum alloy specimen with hole and cylindrical steel core, incipient crack length  $a_0$  and loading  $p_0$

### APPLICATION OF $M$ - AND $L$ -INTEGRALS TO CRACK TIP PLASTIC ZONES

The concept of the configurational forces signifies their vanishing in a defect-free body. Within the framework of the FE-method, however, it is observed that, depending on the applied mesh, configurational forces arise though no defects are existent [23]. This phenomenon may be used for the adaption of FE meshes in terms of vanishing configurational forces at internal nodes [23], and as an error indicator of the FE solution [24]. Our investigations confirm that these configurational forces depend on the mesh and the loading. However, configurational forces in an homogeneous body are small compared to those resulting from defects.

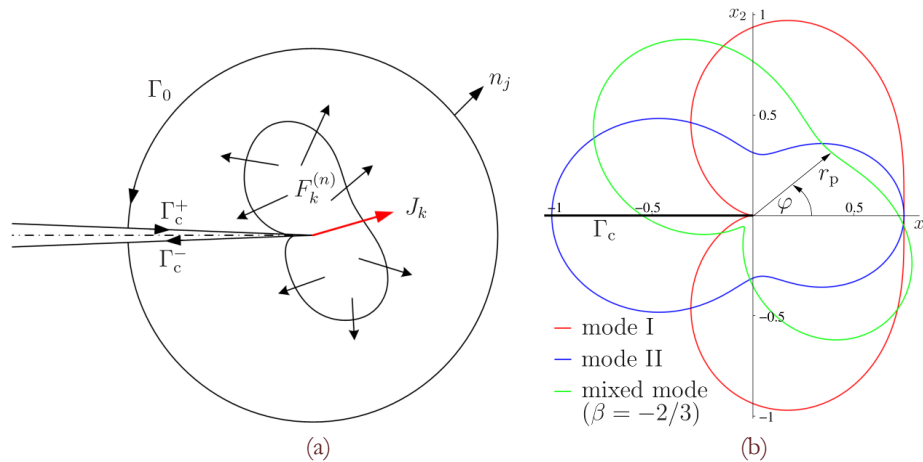


Figure 3: (a) Integration contour  $\Gamma_0$  and  $\Gamma_c$  enclosing the crack tip and the plastic zone, material forces  $F_k^{(n)}$  and the crack driving force  $J_k$ , (b) shapes of crack tip plastic zones in normalized depiction  $r_p(\varphi) / r_p^{\max}$  from the von Mises yield criterion.

A new application of the configurational forces approach is the separation of the crack driving force and the forces acting at a plastic deformation  $F_k^{(n)}$ , see Fig. 3(a). Evaluating the  $M$ - and  $L$ -integrals at remote integration contours e.g. along the external boundaries of the model, as presented in Section 2, the contribution of configurational forces in the crack tip plastic zone in general is implicitly included in the result. In contrast to a global approach of the  $J_k$ -integral, always providing the sum of all configurational forces including  $J_k$  and  $F_k^{(n)}$ , the global approaches of  $M$ - and  $L$ -integrals exclusively represent the contribution of the material forces in the plastic zone, if the origin of the global coordinate system is the crack tip. In that case the crack driving force  $J_k$  has no contribution to  $M$  or  $L$ .

The model of a double cantilever beam (DCB) specimen with different loading conditions is investigated, see Fig. 4(a), including a single mode-I ( $F_1 = F_2 = F$ ), a single mode-II ( $F_1 = -F_2 = 0.5F$ ) and a plane mixed-mode loading with mixed mode ratio  $\beta = K_{II}/K_I = -2/3$  ( $F_1 = F, F_2 = 0$ ). The material model is that of an idealized linear elastic-perfectly plastic behavior with tensile yield strength  $\sigma_y = 462\text{MPa}$ . A first approximation of the plastic zone  $r_p(\varphi)$  is obtained by substituting the closed-form representation of the asymptotic crack tip field into the von Mises yield criterion for the investigated mode cases, leading to the normalized shapes depicted in Fig. 3(b). With this, the extension of the plastic zone  $r_p$  along the ligament is calculated according to

$$d_p = \frac{K_I^2 + 3K_{II}^2}{2\pi\sigma_y^2}, \tag{12}$$

being a simplified measure for the size of the crack tip plastic zone.

The global  $M$ - and  $L$ -integrals are calculated for an increasing load. The calculated values  $M^{pl}$  and  $L^{pl}$  must be corrected considering the initial configurational forces resulting from mesh and external loading. The correction terms are obtained from the global  $M$ - and  $L$ -integrals at the linear-elastic regime, and thus  $\bar{M} = M^{pl} - M^{el}$  and  $\bar{L} = L^{pl} - L^{el}$ . In Fig. 4(b)

corrected  $\bar{M}$  - and  $\bar{L}$  -integrals are plotted vs. the simplified theoretical size of the plastic zone according to Eq. (12). The values are normalized with respect to the maximum values  $\bar{M}^{\max} = 288 \text{ N}$  and  $r_p^{\max} = 4.4 \text{ mm}$  of the mode-I loading case. In Fig. 4(b) it is obvious that the  $M$ -integral increases as the region of the plastic deformation around the crack increases. The mixed-mode crack opening provides negligible values in  $\bar{L}$  compared to  $\bar{M}$  which even remain zero for the mode-I and mode-II crack openings. Nevertheless, the  $L$ -integral may serve as an additional condition describing the distribution of the material forces in the plastically deformed region. These first results seem promising with respect to a new application of the  $M$ - and  $L$ -integrals, separating the crack driving force and the plastic deformation driving forces in a similar manner as the separation of the  $J_k$ -integrals of two interacting cracks [14].

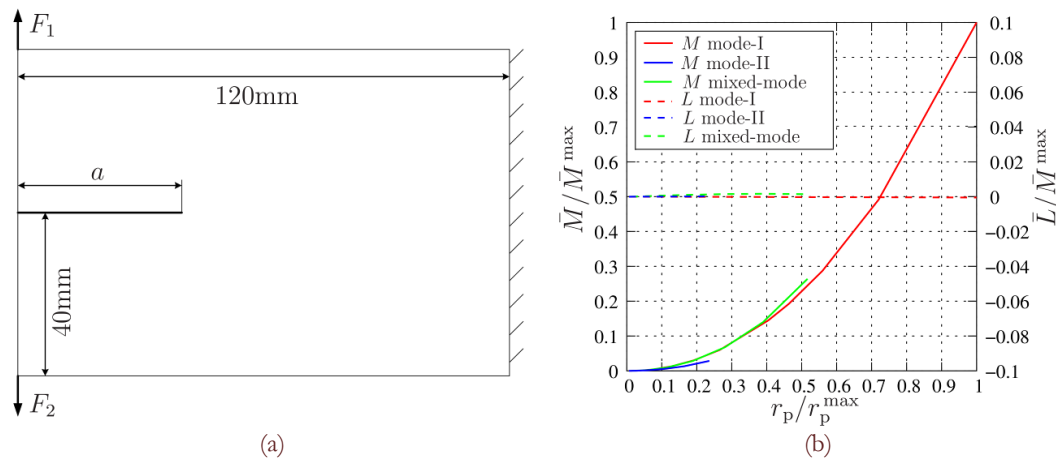


Figure 4: (a) DCB specimen with applied loads  $F_1$  and  $F_2$  and crack length  $a = 40 \text{ mm}$ , (b) normalized global  $M$ - and  $L$ -integrals with a linear elastic-perfectly plastic material model vs. the normalized plastic zone size  $r_p / r_p^{\max}$  from Eq. (12).

## CLOSURE

Path-independent integrals are introduced applying remote integration contours along the external boundaries of the model. This global approach is beneficial compared to a local approach, where small integration contours around the crack tip are applied, as no special requirements regarding the crack tip meshing have to be considered and crack tips approaching interfaces can be appropriately handled. Additional integrals along crack faces, material interfaces and internal boundaries are calculated providing path-independence. It is emphasized, that the integration along material interfaces is important for both, the  $J_k$ - and  $I_k$ -integral for the accurate calculation of the crack tip loading. Crack paths at material interfaces are predicted accurately and compared to experimental findings. Next to the fracture toughness anisotropy, the boundary conditions at a material interface have a strong impact on crack paths. Based on global  $M$ - and  $L$ -integrals, a new approach for the separation of the crack driving force and forces inducing plastic deformation at the crack tip is motivated.

## ACKNOWLEDGEMENT

The authors would like to acknowledge the financial support of the “Landes-Offensive zur Entwicklung Wissenschaftlich-ökonomischer Exzellenz (LOEWE)” Research Funding Program “Safer Materials”.

## REFERENCES

- [1] Eshelby, J.D., The force on an elastic singularity. *Phil. Trans. A*, 244 (1951) 87-112.



- [2] Cherepanov, G.P., Crack propagation in continuous media (translation from russian). *J. Appl. Math. Mech.*, 31 (1967) 503-512.
- [3] Rice, J.R., A path independent integral and the approximate analysis of strain concentration by notches and cracks. *J. Appl. Mech.*, 35 (1968) 379-386.
- [4] Günther, W., Über einige Randintegrale der Elastomechanik. *Abh. Braunschweigischen Wissen. Gesell.*, 14 (1962) 53-72.
- [5] Knowles, J.K., Sternberg, E., On a class of conservation laws in linearized and finite elastostatics. *Arch. Rational Mech. Ana.*, 44 (1972) 187-211.
- [6] Budiansky, B., Rice, J.R., Conservation laws and energy-release rates. *J. Appl. Mech.*, 40 (1973) 201-203.
- [7] Kienzler, R., Herrmann, G., *Mechanics in material space with applications to defect and fracture mechanics*. Springer, Berlin, 2000.
- [8] Bergez, D., Determination of stress intensity factors by use of path-independent integrals. *Mech. Res. Commun.*, 1 (1974) 179-180.
- [9] Eischen, J.W., An improved method for computing the  $J_2$  integral. *Eng. Fract. Mech.*, 26 (1987) 691-700.
- [10] Judt, P.O., Ricoeur A., Accurate loading analyses of curved cracks under mixed-mode conditions applying the  $J$ -integral. *Int. J. Fract.*, 182 (2013) 53-66.
- [11] Stern, M., Becker, E.B., Dunham, R.S., A contour integral computation of mixed-mode stress intensity factors. *Int. J. Fract.*, 12 (1976) 359-368.
- [12] Judt, P.O., Ricoeur, A., Consistent application of path-independent interaction integrals to arbitrary curved crack faces. *Arch. Appl. Mech.*, 85 (2015) 13-27.
- [13] Judt, P.O., Ricoeur, A., Crack growth simulation of multiple cracks systems applying remote contour interaction integrals. *Theo. App. Fract. Mech.*, 75 (2015) 78-88.
- [14] Judt, P.O., Ricoeur, A., A new application of  $M$ - and  $L$ -integrals for the numerical loading analysis of two interacting cracks. *Z. Angew. Math. Mech.*, (2015). doi: 10.1002/zamm201500012.
- [15] Sih, G.C., Paris, P.C., Irwin, G.R., On cracks in rectilinearly anisotropic bodies. *Int. J. Fract. Mech.*, 1 (1965) 189-203.
- [16] Judt, P.O., Ricoeur, A., Linek, G., Crack path prediction in rolled aluminum plates with orthotropic properties and experimental validation. *Engineering Fracture Mechanics*, 138 (2015) 33-48.
- [17] Eischen, J.W., Herrmann G., Energy release rates and related balance laws in linear elastic defect mechanics. *J. Appl. Mech.*, 54 (1987) 388-392.
- [18] Yu, H., Wu, L., Guo, L., Du, S., He, Q., Investigation of mixed-mode stress intensity factors for nonhomogeneous materials using an interaction integral method. *Int. J. Solids Struct.*, 46 (2009) 3710-3724.
- [19] Judt, P.O., Ricoeur, A., Crack growth in elastic materials with internal boundaries and interfaces. In *Proceedings in Applied Mathematics and Mechanics 12* (2012) 159-160, GAMM Tagung, Darmstadt, Germany.
- [20] Patton, E.M., Santare, M.H., Crack path prediction near an elliptical inclusion. *Engineering Fracture Mechanics*, 44 (1993) 195-205.
- [21] Bouchard, P.O., Bay, F., Chastel, Y., Numerical modelling of crack propagation: automatic remeshing and comparison of different criteria. *Comput. Meth. Appl. Mech. Eng.*, 192 (2003) 3887-3908.
- [22] Nielsen, C.V., Legarth, B.N., Niordson C.F., Extended FEM modeling of crack paths near inclusions. *Int. J. Numer. Meth. Eng.*, 89 (2012) 786-804.
- [23] Braun, M., Configurational forces induced by finite-element discretization. *Proc. Estonian Acad. Sci. Phys. Math.*, 46 (1997) 24-31.
- [24] Gross, D., Mueller, R., Kolling, S., Configurational forces - morphology evolution and finite elements. *Mech. Res. Commun.*, 29 (2002) 529-536.